Bioresource Technology 102 (2011) 5757–5763

Contents lists available at ScienceDirect

Bioresource Technology

journal homepage: www.elsevier.com/locate/biortech

Sorption of bisphenol A, 17α-ethinyl estradiol and phenanthrene on thermally and hydrothermally produced biochars

Ke Sun [a,b], Kyoung Ro [c], Mingxin Guo [d], Jeff Novak [c], Hamid Mashayekhi [b], Baoshan Xing [b,*]

[a] State Key Laboratory of Water Simulation, School of Environment, Beijing Normal University, Beijing 100875, China
[b] Department of Plant, Soil, and Insect Sciences, University of Massachusetts, Amherst, MA 01003, USA
[c] USDA-ARS Coastal Plains Soil, Water, and Plant Research Center, 2611 W. Lucas Street, Florence, SC 29501, USA
[d] Department of Agriculture and Natural Resources, Delaware State University, Dover, DE 19901, USA

ARTICLE INFO

Article history:
Received 31 January 2011
Received in revised form 11 March 2011
Accepted 13 March 2011
Available online 17 March 2011

Keywords:
Biochar
Hydrothermal
Endocrine disrupting chemicals
Adsorption
Pyrolysis

ABSTRACT

Thermal and hydrothermal biochars were characterized, and adsorption of bisphenol A (BPA), 17α-ethinyl estradiol (EE2) and phenanthrene (Phen) was determined to investigate the sorption characteristic difference between the two types of biochars. Thermal biochars were composed mostly of aromatic moieties, with low H/C and O/C ratios as compared to hydrothermal ones having diverse functional groups. Single-point organic carbon-normalized distribution coefficients ($\log K_{OC}$) of EE2 and BPA of hydrothermal biochars were higher than thermal biochars, while Phen $\log K_{OC}$ values were comparable among them. X-ray diffraction and solid state nuclear magnetic resonance results suggested that hydrothermal biochars consisted of more amorphous aliphatic-C, possibly being responsible for their high sorption capacity of Phen. This study demonstrated that hydrothermal biochars could adsorb a wider spectrum of both polar and nonpolar organic contaminants than thermally produced biochars, suggesting that hydrothermal biochar derived from poultry and animal waste is a potential sorbent for agricultural and environmental applications.

1. Introduction

Biochars, byproducts of the pyrolytic processing of organic feedstocks, are attracting international attention for the following three reasons. First, biochars can be used as soil amendments for improving soil properties and crop yield (Chan et al., 2008; Sohi et al., 2010); second, storing biochars in soils along with bioenergy production is regarded as an effective means for sequestering carbon (C) to mitigate climate change (Lehmann et al., 2006); and third, biochar in soil is recognized as an effective sorbent for potentially hazardous organic compounds (Cao et al., 2009; Yu et al., 2009). However, the ability of biochar to store C and improve soil fertility depends on its physical and chemical properties, which vary greatly with the pyrolysis process conditions and feedstock source (Liang et al., 2008; Novak et al., 2009). Because degraded soils in different regions around the world have various quality issues, one type of biochar will not solve all soil quality problems. It has been reported that biochars composed of mostly aromatic-C may best be suited for carbon-sequestering soil amendments because of their recalcitrant nature (Liang et al., 2008; Novak et al., 2009; Glaser et al., 2002); these biochars with large amounts of condensed aromatic C are generally obtained by pyrolyzing feedstock at high temperature (400–700 °C) (Liang et al., 2008). However, they have fewer ion exchange functional groups (Novak et al., 2009). On the other hand, biochars produced at lower temperature (250–400 °C) have higher yields and contain more diversified characteristics (Novak et al., 2009; Glaser et al., 2002; Keiluweit et al., 2010; Chen et al., 2008). Addition of low-temperature biochars to soils is reported to improve soil fertility by raising soil cation exchange capacity due to carboxylic groups on their own surface and to exposed carboxylic groups of organic acids sorbed by the biochars, both contributing negative surface charges (Liang et al., 2006). Recalcitrant characteristics of high-temperature biochar would be a desirable property if the primary purpose was to remove atmospheric CO_2 by sequestering biomass-C in soil. Low-temperature biochars will probably be more suitable to improve soil fertility than high-temperature biochars due to both the relatively stable aromatic backbone from pyrolysis and more C═O and C—H functional groups which may serve as nutrient exchange sites after oxidation (Novak et al., 2009; Glaser et al., 2002). Moreover, biochars could adsorb hazardous organic compounds as indicated from previous studies (Cao et al., 2009; Yu et al., 2009; Liang et al., 2008; Chen et al., 2008).

Much work has been done on plant-residue and animal-waste derived biochars for sorbing organic pollutants (Chan et al., 2008; Cao et al., 2009; Chun et al., 2004). For example, Cao et al. (2009) showed that dairy manure can be converted into biochar to sorb me-

* Corresponding author. Tel.: +1 413 545 5212; fax: +1 413 545 3958.
E-mail address: bx@pssci.umass.edu (B. Xing).

0960-8524/$ - see front matter © 2011 Elsevier Ltd. All rights reserved.
doi:10.1016/j.biortech.2011.03.038

tal and/or organic contaminants; Yang and Sheng (2003) reported that soil amended with rice or wheat-straw derived biochar enhanced sorption of diuron and atrazine. Compared to high-temperature biochars, biochars obtained at low temperature (below 300 °C) generally exhibit low sorption capacity, especially for hydrophobic organic contaminants (HOCs) (Chen et al., 2008; Wang and Xing, 2007). The high-temperature biochars are particularly effective in sorption and sequestration of organic contaminants in soil due to their greater surface area within aromatic components and high microporosity (Chen et al., 2008; Chun et al., 2004). However, they contain too little aliphatic carbons and functional groups to improve soil fertility to large extent, due to functional groups being as nutrient exchange sites and aliphatic carbons serving as substrates for mineralization by bacteria and fungi as mentioned above (Glaser et al., 2002; Novak et al., 2009). Therefore, it would be ideal to produce biochars which not only contain functional groups to serve as nutrient exchange sites (Glaser et al., 2002), but also have high sorption capacity for organic compounds.

The volume of animal manures in many countries shows a sustained and increasing trend, e.g. in UK the poultry farming industry produces 1.5 million tons per year (Dávalos et al., 2002) and in USA animal production annually provides 35 million tons of sustainable biomass (Perlack et al., 2005; Cantrell et al., 2008). These animal manures can be carbonized to produce carbonaceous solids either by dry pyrolysis or hydrothermal carbonization techniques.

Hydrothermal carbonization is a relatively rapid method to produce biochars in the presence of water. During hydrothermal carbonization, biomass is heated in subcritical water to between 150 and 350 °C at autogenic pressures for reaction time frames typically greater than 1 h. Feedstock decomposition is initiated with hydrolysis and subsequently dominated by reaction mechanisms such as dehydration, decarboxylation, aromatization, and recondensation (Funke and Ziegler, 2010). The advantage of hydrothermal carbonization is that it can convert wet feedstocks such as swine and dairy manures into carbonaceous solids at relatively high yields without the need of an energy intensive drying before or during the process.

Endocrine disrupting chemicals (EDCs) can mimic the biological activity of natural hormones, occupy hormone receptors, or interfere in the transport and metabolic processes of natural hormones (de Rudder et al., 2004). The main source of EDCs in the environment is municipal sewage. EDCs were detected in the effluents of sewage treatment plants (Hu et al., 2007). Due to the shortage of water resources in many regions in the world, effluents from wastewater treatment plant after biological processes have been widely used for agricultural irrigation (Chen et al., 2005). As a result, EDCs would accompany effluents and land application of biosolids to enter into soils. If biochars are added to soil to improve fertility and store C: there is a potential for biochars and EDCs interaction. This study investigated the sorption characteristics of EDCs on biochars. There is little information in the literature examining interactions of biochars with EDCs, especially biochars produced using different processes (dry pyrolytic vs. hydrothermal). Therefore, the specific objectives of this study were: (1) to investigate the influence of thermal and hydrothermal methods and feedstock selection on both physical and chemical properties of biochars and their sorption behavior of polar and apolar aromatic compounds, and (2) to examine possible sorption mechanisms of the selected organic chemicals by the biochars.

2. Methods

2.1. Sorbates

17α-Ethinyl estradiol (EE2) and bisphenol A (BPA) are two of the most frequently studied EDCs in environmental research. As the solubility of BPA in water is 50 times higher than EE2 and thus, the two chemicals could represent EDCs with a wide range of water solubility. Phenanthrene (Phen), a polycyclic aromatic hydrocarbon, is ubiquitous in the environment. Analytical-grade BPA and EE2 were obtained from Aldrich Co. (Milwaukee, WI). ^{14}C-labeled and unlabeled Phen were purchased from Sigma–Aldrich Chemical Co. Selected physicochemical properties of BPA, EE2, and Phen are presented in Table S1 (Supplementary data).

2.2. Sorbents

The two thermal biochars T-PL and T-WS were produced from feedstocks of poultry litter and wheat straw, respectively, through pyrolysis at 400 °C until no visible smoke was emitted from the reactor (120–420 min). They were washed with 0.1 M HCl followed by water till neutral pH, subsequently oven-dried at 105 °C, gently ground, and homogenized to pass through a 250 μm sieve.

Two hydrothermal biochars (H-SS and H-PL) were produced by carbonizing poultry litter and swine solids in tubular stainless steel reactors. In each of ten 180 mL tubular stainless steel reactors, 11.6 g of swine solids or poultry litter were mixed with 45 mL deionized water to make 20.5% solid feedstock. These tubular reactors were loaded into a Lindberg bench furnace (Lindberg/Blue M with retort, Wateron, WI). Slurry feedstock was carbonized at 250 °C under autogenic pressures for 20 h. After cooling overnight, the reactors were opened and 80 mL acetone was added into each reactor. The reactors were reclosed and shaken for 3 h to extract tarry materials deposited on hydrothermal biochar. Then, hydrothermal biochars were separated from liquid (acetone + water) using Whatman 934-AH glass microfiber filter paper. The separated biochars were dried at 105 °C, gently ground and homogenized to pass through a 250 μm sieve. Because biochars were produced at 250 °C in the presence of water, they were named hydrothermal biochars to distinguish them from the thermal ones produced at 400 °C without water.

2.3. Biochar characterization

The C, H, and N contents of the biochars were determined using an Elementar Vario ELIII elemental analyzer. Elemental composition was measured in duplicate, with the averaged data were reported. Ash content was measured by heating the samples at 750 °C. The O content was calculated by mass difference. Fourier transform infrared (FTIR) spectra of the samples were obtained using a Perkin–Elmer spectrometer (Spectrum One) with a diffuse-reflectance sampling accessory (Waltham, MA). Solid-state cross-polarization magic-angle-spinning ^{13}C NMR spectra were obtained using a Bruker DSX-300 spectrometer (Karlsruhe, Germany). The NMR running parameters and chemical shift assignments are depicted elsewhere (Ran et al., 2007). Pore and surface characteristics were examined by gas adsorption using an Autosorb-1 gas analyzer (Quantachrome Instrument Corp., Boynton Beach, FL). Surface area (SA-CO_2), pore volume, pore size, and pore size distribution using CO_2 isotherm at 273 K were calculated using nonlocal density functional theory (NLDFT) and grand canonical Monte Carlo simulation (GCMC) (Braida et al., 2003). The surface area using N_2 (SA-N_2) was determined by the Brunaer–Emmett–Teller (BET) equation with multipoint adsorption isotherms of N_2 at 77 K. Also, X-ray diffraction (XRD) patterns were recorded using an X'Pert PRO MPD diffractometer (PANalytical, Holland) with Cu Kα radiation at 40 mA and 40 kV. The diffractometer was operated with a step size of 2θ (0.02°).

2.4. Sorption experiments and detection of EE2, BPA and Phen

Sorption isotherms were obtained using a batch equilibration technique as described previously (Ran et al., 2007). Briefly, so-

lid-to-solution ratios were adjusted to obtain 30–80% solute uptake by sorbents. The background solution contained 0.01 M $CaCl_2$ to maintain a constant ionic strength and 200 mg L^{-1} of NaN_3 to inhibit microbial activity. Test solutions of various solute concentrations (with 100–4000 μg L^{-1} for EE2, 25–12,000 μg L^{-1} for BPA, and 10–1120 μg L^{-1} for Phen) were prepared by introducing stock solutions of the solutes to the background solution. After being shaken for overnight, the test solutions were added to the sorption vials with predetermined amounts of sorbents until a minimum headspace was achieved. The vials were immediately sealed with Teflon screw caps and then placed on a rotary shaker to mix for 7 days at 23 ± 1 °C. Our preliminary test indicated that apparent equilibrium was reached within 7 days for the biochars. After mixing, the vials were centrifuged at 3000 rpm for 30 min, and 0.8 mL of Phen supernatant was sampled and added to ScintiVerse cocktail (6 mL; Fisher Scientific) for liquid scintillation counting (Ran et al., 2007). For EE2 and BPA, supernatant was transferred to a 2 mL vial and analyzed using HPLC (HP model 1100, reversed phase C18, 250 cm × 4.6 mm × 4.6 μm). The mobile phase was 60:40 (v:v) of acetonitrile and deionized water with 1% acetic acid. Concentration of EE2 was analyzed with a fluorescence detector at 206 nm (excitation wavelength) and 310 nm (emission wavelength), while BPA was quantified on a fluorescence detector at 228 nm (excitation wavelength) and 316 nm (emission wavelength) for the concentration range of 25–4000 μg L^{-1}, and on a UV detector at 280 nm for the samples with concentrations higher than 4000 μg L^{-1}. Each isotherm consisted of 10 solute concentration levels. All samples, along with blanks, were run in duplicate. Because the mass loss of solute was negligible, adsorption of solutes by biochars was determined by mass balance.

2.5. Data analysis

Freundlich model (FM) was used to fit the sorption data.

$$\log q_e = \log K_F + n \log C_e \quad (1)$$

where q_e (μg g^{-1}) is the equilibrium sorbed concentration; C_e (μg L^{-1}) is the equilibrium aqueous concentration; K_F (μg g^{-1}/(μg $L^{-1})^n$) is the Freundlich affinity coefficient; and n is the Freundlich exponential coefficient. Dubinin–Ashtakhov (DA) model instead of Polanyi-Manes model (PMM) was employed to fit the adsorption isotherms because molar volume (V_s) was used as a constant in the regression analysis even though V_s value of the compounds could not be given.

$$\log q_e = \log Q^0 - (\epsilon/E)^b \quad (2)$$

where Q^0 (mg g^{-1}) is the saturated adsorption capacity; $\varepsilon = RT\ln(C_s/C_e)$ is the effective adsorption potential (kJ mol^{-1}); C_s (mg L^{-1}) is the water solubility at 20 °C (7.6 mg L^{-1} for EE2, 380 mg L^{-1} for BPA, and 1.12 mg L^{-1} for Phen); R (8.314 × 10^{-3} kJ/(mol K)) is the universal gas constant; and T (K) is absolute temperature; E (kJ mol^{-1}) is the "correlating divisor"; and b is the fitting parameter.

3. Results and discussion

3.1. Characteristics of biochars

The elemental composition of hydrothermal biochars (H-PL and H-SS) and thermal biochars (T-PL and T-WS) is listed in Table 1. Organic carbon (OC) contents (53.5–65.8%) of thermal biochars were higher than the hydrothermal ones (40.2–47.5%). The H/C ratios of 0.83 and 0.63 for T-PL and T-WS, and of 1.45 and 1.15 for H-SS and H-PL, respectively, indicate thermal biochars were more carbonized than H-SS and H-PL. In addition, higher than unity H/C ratio (>1.0) suggests that H-SS and H-PL may contain a good amount of original organic residues, such as polymeric CH_2, lignin, and cellulose (polar fractions) (Novak et al., 2009; Keiluweit et al., 2010; Chen et al., 2008); while lower H/C ratios indicate that T-PL and T-WS were highly thermally altered unsaturated material after dehydration (Keiluweit et al., 2010). The H/C and O/C atomic ratios in this study and other literature data were plotted in a typical van Krevelen diagram (Fig. S1). The major components of H-PL, H-SS and the reported biochars from low-temperature (200–250 °C) were lignin-type molecules; while, T-PL, T-SS and the reported biochars from high-temperature were more like coal and char-type molecules. As a result, major components of the two types of biochars were substantially different. The hydrophobicity and condensation of the thermal biochars were higher than hydrothermal ones due to the progressive decrease in the H/C and O/C atomic ratios with temperature associated with dehydration reaction, also supported by the previous results that low-temperature biochars generally had high H/C ratio and were mainly composed of lignin and cellulose, while high-temperature biochars consisted of condensed aromatic-rich moieties with the H/C and O/C atomic ratios (Novak et al., 2009; Keiluweit et al., 2010).

SA-N_2 (77 K, BET) of the four biochars ranged from 2.1 to 8.8 m^2 g^{-1} (Table 1). The correlation analysis between SA-N_2 of the four biochars and their ash content showed that the SA-N_2 increased with increasing ash content (Table 1 and Fig. S2a), suggesting the SA-N_2 may primarily only represent the surface on the minerals in the biochars. The SA-CO_2 of the four biochars, nevertheless, was much higher (27.2–223 m^2 g^{-1}) than their respective SA-N_2 values. In addition, the SA-CO_2 of the two thermal biochars was much higher than that of the two hydrothermal ones with their ranges of 110–230 and 27.2–61.4 m^2 g^{-1}, respectively. Pore size distribution profile (Fig. 1) indicates that the biochars were highly microporous: nearly all porosity results from pores with diameters <1.5 nm. Most pores of T-PL and T-WS were distributed in the range of 0.4–0.6 nm, accounting for about 57–66% of cumulative pore volume up to 1.5 nm. However, pores of the hydrothermal biochars were scattered in the range of 0.4–1 nm (Fig. 1). Pore size based on GCMC method of the four biochars ranged from 0.42 to 0.79 nm (Table 1).

The FTIR spectra of the four biochars are illustrated in Fig. 2a. The peak assignments are methyl C—H stretching compounds (~2930 cm^{-1}), methylene C–H stretching (~2860 cm^{-1}), aromatic

Table 1
Elemental composition, aromatic ratio, ash content, aromaticity, BET-N2 surface area (SA-N_2), cumulative surface area (SA-CO_2), cumulative pore volume, and pore size.

Samples	C (%)	H (%)	N (%)	O (%)	C/N	H/C	O/C	Ash (%)	H_2O (%)	Aromaticity (%)[a]	SA-N_2[b] (m^2/g)	SA-CO_2[c] (m^2/g)	Pore volume[c] (cm^3/g)	Pore size[c] (nm)
H-SS	47.46	5.72	1.25	20.7	44.35	1.45	0.33	24.9	2.4	33.9	4.03	27.2	0.010	0.79
H-PL	40.20	3.86	1.67	22.1	28.01	1.15	0.41	32.2	2.7	32.8	8.77	61.4	0.021	0.57
T-PL	53.45	3.71	2.80	15.0	22.30	0.83	0.21	25.0	2.9	72.4	6.71	110.2	0.035	0.48
T-WS	65.79	3.43	0.21	20.4	370.50	0.63	0.23	10.2	3.8	81.6	2.08	229.8	0.068	0.42

[a] Aromaticity = 100 × aromatic C(108–165 ppm)/[aromatic C (108–165 ppm) + aliphatic C(0–108 ppm)], the data of aromatic C (108–165 ppm) and aliphatic C (0–108 ppm) are listed in Table S2.
[b] Calculated using the Brunaer–Emmett–Teller (BET) equation for data in the range from 0.05 to 0.3 of relative pressure.
[c] Calculated from nonlocal density functional theory (NLDFT) and grand canonical Monte Carlo simulation (GCMC) using CO_2 adsorption.

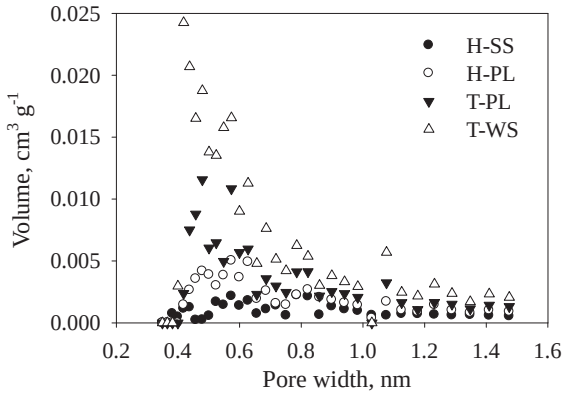

Fig. 1. Pore size distributions of hydrothermal (H-SS and H-PL) and thermal (T-PL and T-WS) biochars measured by CO_2 adsorption.

carbonyl/carboxyl C=O (~1700 cm^{-1}), and aromatic C=C (~1600 cm^{-1}) (Ran et al., 2007). Signals at 1180–1030 cm^{-1} in hydrothermal biochars may arise from the C–H deformation of cellulose-derived substituted aromatics (Pastorova et al., 1994), and the peak of 885–752 cm^{-1} is assigned to the aromatic C–H out-of-plane deformation (Haberhauer et al., 1998). The H-SS had the strongest signal of the aliphatic group (~2930 and ~2860 cm^{-1}) among all biochars. The aromatic groups (~1600, ~1700, and 885–752 cm^{-1}) of the two thermal biochars were stronger than that of the two hydrothermal ones (Fig. 2a) due to a higher charring temperature.

The ^{13}C NMR spectra of two types of biochars were very different in functional groups (Fig. 2b). The NMR spectra for the thermal biochars reveal a large contribution from aryl carbon (108–148 ppm), especially for T-WS, and a small contribution from alkyl carbon (0–45 ppm) but negligible contribution from other structural groups. In contrast, the ^{13}C NMR spectra of hydrothermal biochars show a larger contribution from alkyl carbon (0–45 ppm) (for H-SS), methoxyl carbon (45–63 ppm), carbohydrate (63–108 ppm), *O*-aryl (148–165 ppm), and carboxyl carbon (165–187 ppm) (Fig. 2b). The aromaticity of T-WS and T-PL was 81.6% and 72.4%, respectively. However, the aromaticity of hydrothermal biochars was clearly lower than the thermal biochars with their values being 33.9% and 32.8%, respectively. It is noted that the NMR spectrum of H-PL in this study was very similar to a biochar made from switchgrass at 250 °C (Novak et al., 2009); however, the H-PL had the relatively large broadening of most signals compared to switchgrass at at 250 °C which had separate peaks (Fig. 2 and Fig. S6), suggesting that C of H-PL as well as H-SS may be derived from unordered molecular structure of lignin, hemicelluloses and amorphous cellulose region (Nogueira et al., 2004). NMR spectrum of a poultry litter biochar made at 350 °C in a previous work was also similar to that of T-PL in this study (Fig. 2b and Fig. S6).

The XRD patterns of the four biochars are shown in Fig. 3. Sharp and strong peaks in the four biochars especially for H-PL, T-PL, and T-SW indicate miscellaneous inorganic components mainly are composed of quartz. At the same time, the four biochars showed elevated background between $2\theta = 14–26$ °C, likely attributable mainly to organic matter (Fig. 3) (Cao and Willie, 2010), however, the lack of peaks at 0.60, 0.53, 0.404, and 0.59 nm, which are assigned to crystallographic planes of completely ordered regions of cellulose (Keiluweit et al., 2010), respectively, suggests that the organic C of the hydrothermal biochars (H-PL and H-SS) produced at 250 °C would be amorphous, which was not in accordance with thermal biochars produced at 200 and 300 °C mainly consisting of crystallographic planes of ordered regions of cellulose (Keiluweit et al., 2010). On the other hand, the thermal biochars possibly consist of entirely random and disintegrated C phase but turbostratic carbon crystallites due to the absence of peaks at around 0.381 and 0.207 nm (assigned to turbostratic carbon crystallites) on their XRD pattern (Fig. 3). Previous research found the existence of an intermediate, amorphous C stage within the narrow temperature interval 410–450 °C (Paris et al., 2005) and 300–400 °C (Keiluweit et al., 2010), respectively, when wood or grass were heated at different charring temperatures.

Although H-PL and T-PL started with similar feedstock materials, significant difference in functional groups, surface properties, and elemental composition were observed (Table 1 and S2, Fig. S1) and should be mainly due to different pyrolysis processing conditions they were subjected. On the other hand, when a pyrolysis method was used, feedstock selection also had a substantial influence on biochar properties; while alkyl C (0–45 ppm) of H-

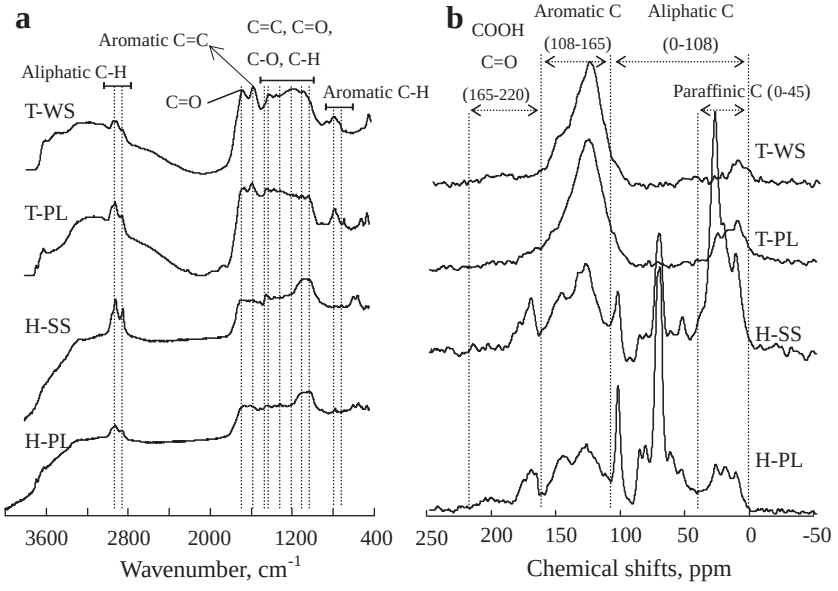

Fig. 2. Fourier transform infrared (FTIR) spectra (a) and ^{13}C nuclear magnetic resonance (NMR) spectra (b) of hydrothermal (H-SS and H-PL) and thermal (T-PL and T-WS) biochars.

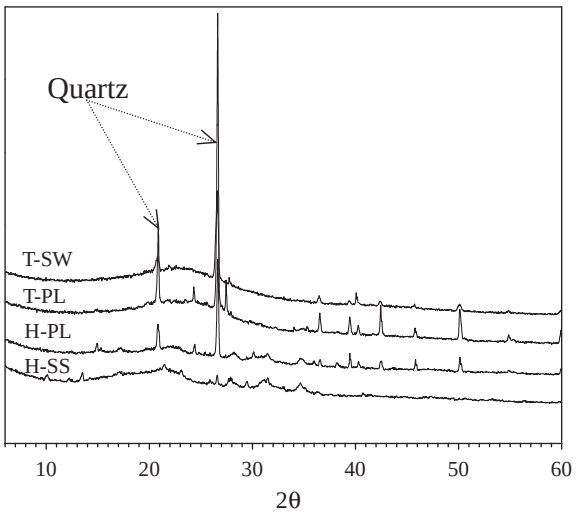

Fig. 3. XRD patterns of hydrothermal (H-SS and H-PL) and thermal (T-PL and T-WS) biochars.

SS was remarkably high while O-alkyl C (63–108 ppm) was low, H-PL had high O-alkyl C and low alkyl C (Fig. 2, Table S2). In addition, difference in surface properties was observed for the biochars produced from different feedstock materials but from the same processing condition as reflected in SA-CO_2 between H-PL and H-SS and similarly between T-WS and T-PL (Table 1).

3.2. Sorption isotherms of BPA, EE2, and Phen

All sorption isotherms of EE2 and BPA were highly nonlinear as evident from Freundlich exponents (n) being from 0.37 to 0.80. However, Phen isotherms of hydrothermal biochars were less nonlinear than the thermal ones with n being in the range of 0.75–0.91 and 0.60–0.67 for hydrothermal and thermal biochars, respectively (Table S3). The logK_{OC} values of biochars in low concentrations (Table S3) can be obtained by dividing q_e/C_e ($C_e = 0.005\ S_W$) by the f_{oc} values (Table 1). The logK_{OC} value varied with the different equilibrium concentrations due to nonlinear isotherm. Phen K_{OC} values of both thermal and hydrothermal biochars were similar to that of biopolymer-derived chars obtained at 400 °C (Wang and Xing, 2007). It was also reported that these high-temperature biochars are effective in sorption and sequestration of organic contaminants in soil (Chen et al., 2008; Chun et al., 2004). For example, Chen et al. (2008) found that the biochar produced at 400 °C exhibited higher adsorption capacity to both polar and nonpolar aromatic compounds (naphthalene, nitrobenzene, and *m*-dinitrobenzene) than another biochar produced at 250 °C, which was different from our results that the hydrothermally produced biochars generally exhibited higher or similar sorption to both polar and nonpolar compounds (BPA, EE2, and Phen) than high-temperature ones (Fig. 4). The above inconsistency was most likely resulted by the different C phases. Aliphatic groups of thermal biochars produced at 250 °C in this study were mainly composed of poorly crystalline C based on the above characterization by XRD (Fig. 3), while other thermal biochars derived from plants at low temperature possibly contained majority of crystalline C according to the result reported by Keiluweit et al. (2010).

The fitting results of the adsorption isotherms using DA model are listed in Table S4. EE2 OC-normalized adsorption capacity Q^0_{OC} (917) of H-SS was far higher than the maximum of OC-normalized q_e (61.2) calculated based on its Freundlich parameters (n and K_{FOC}) (Table S3) when $C_e = S_W$ (solubility of EE2) in water (Table S1). Therefore, the unreasonably high EE2 Q^0_{OC} and low

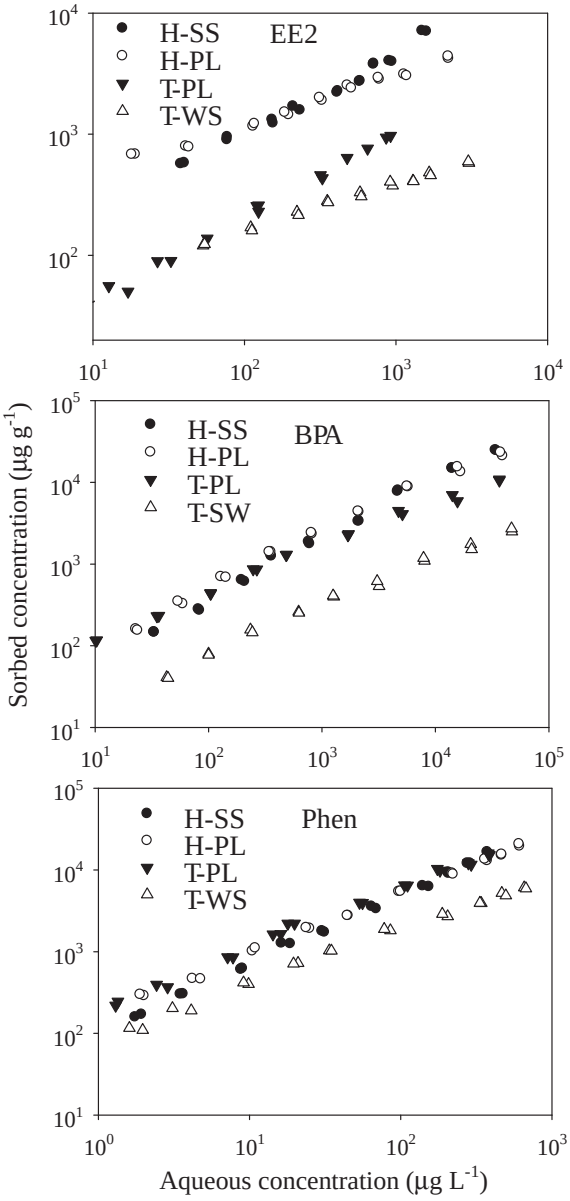

Fig. 4. Sorption isotherms of 17α-ethinyl estradiol (EE2), bisphenol A (BPA), and phenanthrene (Phen) by thermal (T-PL and T-WS) and hydrothermal (H-SS and H-PL) biochars.

parameter b (0.40), being far lower than 1, of H-SS from DA model (Table S4) may result from unreliable extrapolation of the adsorption isotherms. Thus, the following discussion excludes this data.

3.3. BPA and EE2 sorption difference between hydrothermal and thermal biochars

Our above results showed that the hydrothermal biochars produced at 250 °C in the presence of water had higher sorption to EE2 and BPA than the thermal biochars (Fig. 5a). Elemental composition and structural characteristics of biochars possibly play a dominant function in their sorption behavior. First, more polar functional groups and higher O/C ratios in hydrothermal biochars (Table 1 and Fig. 2) imply that the polarity of the hydrothermal biochars was higher than that of the thermal biochars due to contributing little of N/C ratio to the polarity index (O + N/C) resulted by negligible content of N (Table 1). Moreover, a positive relation-

ship between polarity (O/C) and the logK_{OC} values was observed for both EE2 and BPA, especially for EE2 (*Fig.* S2b): it suggests that polar functional groups of the hydrothermal biochars are important in sorption of EE2 and BPA. In addition, overall positive correlations were observed between the logK_{OC} values of EE2 or BPA and aliphatic components of the sorbents (*Fig.* S2c), indicating that polarity and aliphatic carbons could be interactive parameters to regulate the sorption of BPA and EE2.

3.4. Comparable Phen sorption capacity but different nonlinearity n values between hydrothermal and thermal biochars

Although O/C ratios of the hydrothermal and thermal biochars were quite different, both had comparable logK_{OC} for nonpolar Phen. However, their isotherm nonlinearity *n* values (ranging from to 0.60 to 0.91) were different. Thermal biochars exhibited stronger nonlinearity than hydrothermal biochars (Table S3). It is suggested that aromatic domains do not necessarily govern the sorption capacity (K_{OC}) of Phen: however, they contribute to the nonlinearity, which was probably due to nanovoids present within the condensed aromatic domains (Zhu and Pignatello, 2005). Hydrothermal biochars contained mainly aliphatic components while thermal biochars had high contents of aromatic carbons (Table S2). Moreover, there was a good positive relationship between *n* and pore size of the four biochars (Fig. S3). The fact that aromatic domain of the thermal biochars led to strong nonlinear sorption, but not significantly higher Phen sorption (K_{OC}) than aliphatic domains within hydrothermal biochars (Zhu and Pignatello, 2005) suggests different sorption domains taking place in the two types of biochars. The comparable sorption capacity of hydrothermal biochars from low temperature with the thermal ones produced at high temperature in this study or the condensed NOM samples (Ran et al., 2007) should be attributed to the amorphous C within hydrothermal biochars according to their XRD pattern (Fig. 3). A recent review also suggested that the mobile amorphous aliphatic regions are considered as an ideal environment for the partitioning of HOCs (Chefetz and Xing, 2009). Therefore, it can be concluded that the amorphous aliphatic regions within hydrothermal biochars and aromatic moieties of thermal biochars may be responsible for their respective high sorption capacity of Phen.

3.5. Potential sorption mechanism of Phen, EE2, and BPA

The logK_{OC} values of Phen, EE2, and BPA for each biochar (T-PL, T-WS, H-SS, and H-PL) followed an order at any test concentrations of three solutes: Phen > EE2 > BPA, similar to the order of their hydrophobicity (K_{OW} in Table S1). The K_{OC} values were normalized with octanol–water partition coefficient (K_{OW}) to investigate other sorption mechanisms besides hydrophobic effect. After K_{OW} normalization, BPA had the highest logK_{OC}/logK_{OW} for any given biochar (Table S3 and Fig. 5b), indicating that there would be other influencing factors such as the sorbate's dimension or arrangement of functional groups. Otherwise, logK_{OC}/logK_{OW} values of the three sorbates would be comparable.

Previous studies showed that pore-filling is one of dominant sorption mechanisms for HOCs to pyrolyzed chars (Chun et al., 2004). In this study, it was noted that the order of increasing logK_{OC}/logK_{OW} ratio of the four biochars generally agreed with the order of decreasing critical molecular diameter of three sorbates. Also, the saturated adsorption capacity (Q^0_{OC}) based on the DA model increased with increasing pore size of four biochars (Fig. S5A, S5B, and S5C). These findings lead to the pore-filling mechanism for BPA, EE2, and Phen sorption in the biochars. Similar results were also reported by others (Chun et al., 2004). However, there was no positive relationship between logK_{OC}/logK_{OW} vs. SA-CO_2 nor Q^0_{OC} vs. pore volume-CO_2 (Fig. S5D). This non-positive relationship suggests additional mechanisms for EE2, BPA, and Phen adsorption by the four biochars. For thermal biochars with high aromaticity, high logK_{OC}/logK_{OW} of BPA might be attributed to strong π–π EDA interaction with BPA as π-donor (–OH substituted aromatic compounds) (Fig. S4). It has been also reported that the polarity and structure of polar aromatic compounds may fit better with the exposed polar aromatic cores in biochars than Phen (Zhu et al., 2004). Moreover, BPA has the strongest ability to provide the donors due to its two benzene rings (with two phenol groups) (Fig. S4), and more access to sorption sites because of its smallest molecular size. Further, H-bonding interaction could occur especially for sorbates and sorbents with polar functional groups (Crittenden et al., 1999). Hydrothermal biochars would have a high potential for H-bonding accepting or donating owing to their numerous O-containing functional groups. According to their H-bonding acceptor or donor parameters (Table S1), EE2 and BPA can serve as both H-bonding acceptor and H-bonding donor like atrazine (Sun et al., 2010). Though H-bonding acceptor or donor parameters of Phen were calculated to be zero, it was reported that the rings of Phen could act as a weak H-bonding acceptor due to the absence of hydroxyl group (Zhu et al., 2004). Therefore, Phen sorption by the hydrothermal biochars may occur through weak π–H-bonding interactions between the rings of Phen and H-bonding donor groups of H-SS and H-PL (Zhu et al., 2004). In contrast, H-bonding should be minimal in Phen sorption by the thermal biochars due to their low content of functional groups as compared to the hydrothermal biochars. Previous studies also suggested minimal role of H-bonding in aromatic compound sorption by chars (Sander and Pignatello, 2005). The positive relationship between polarity and BPA or EE2 K_{OC} values, especially between polarity

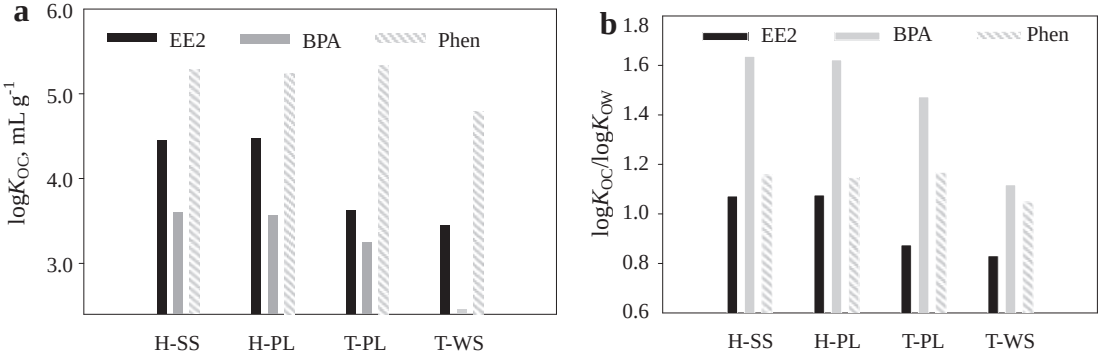

Fig. 5. Comparison of logK_{OC} (a) or logK_{OC}/logK_{OW} ratio (b) between thermal biochars (T-PL and T-WS) and hydrothermal biochars (H-SS and H-PL) for three sorbates: 17α-ethinyl estradiol (EE2) (black bar), bisphenol A (BPA) (grey bar), and phenanthrene (Phen) (diagonal bar).

and EE2 K_{OW}-normalized sorption ($\log K_{OC}/\log K_{OW}$) (Fig. S2b) further supports the importance of H-bonding interactions for BPA and EE2 sorption with the four biochars particularly the hydrothermal biochars due to their higher O-functional group content.

4. Conclusions

Hydrothermal biochars could effectively adsorb both polar and nonpolar compounds due to their diverse structures and functional groups. Therefore, they can serve as effective environmental adsorbents to prevent leaching of organic contaminants, and provide C-substrate to support diverse soil microbial communities. Furthermore, these biochars could increase soil cation exchange capacity to improve soil quality. More importantly, less energy is needed to carbonize wet feedstocks because prior drying is not required in comparison with conventional pyrolysis (Peterson et al., 2008). Thus, hydrothermally produced biochars from poultry and animal-manures have potential for environmental remediation and a new market for manures.

Acknowledgements

This research was supported by the NSF of China (40803029; 50909102), National Basic Research Program of China (2007CB407302), USDA-AFRI (2009-35201-05819), and USDA-NIFA Program (MAES00982).

Appendix A. Supplementary data

Supplementary data associated with this article can be found, in the online version, at doi:10.1016/j.biortech.2011.03.038.

References

Braida, W.J., Pignatello, J.J., Lu, Y.F., Ravikovitch, P.I., Neimark, A.V., Xing, B.S., 2003. Sorption hysteresis of benzene in charcoal particles. Environ. Sci. Technol. 37, 409–417.

Cantrell, K.B., Ducey, T., Ro, K.S., Hunt, P.G., 2008. Livestock waste-to-bioenergy generation opportunities. Bioresour. Technol. 99, 7941–7953.

Cao, X., Ma, L., Gao, B., Harris, W., 2009. Dairy-manure derived biochar effectively sorbs lead and atrazine. Environ. Sci. Technol. 43, 3285–3291.

Cao, X., Willie, H., 2010. Properties of dairy-manure-derived biochar pertinent to its potential use in remediation. Bioresour. Technol. 101, 5222–5228.

Chan, K.Y., Van Zwieten, L., Meszaros, I., Downie, A., Joseph, S., 2008. Using poultry litter biochars as soil amendments. Aust. J. Soil Res. 46, 437–444.

Chefetz, B., Xing, B., 2009. Relative role of aliphatic and aromatic moieties as sorption domains for organic compounds: a review. Environ. Sci. Technol. 43, 1680–1688.

Chen, B., Zhou, D., Zhu, L., 2008. Transitional adsorption and partition of nonpolar and polar aromatic contaminants by biochars of pine needles with different pyrolytic temperatures. Environ. Sci. Technol. 42, 5137–5143.

Chen, Y., Wang, C., Wang, Z., 2005. Residues and source identification of persistent organic pollutants in farmland soils irrigated by effluents from biological treatment plants. Environ. Int. 31, 778–783.

Chun, Y., Sheng, G., Chiou, C.T., Xing, B., 2004. Compositions and sorptive properties of crop residue-derived chars. Environ. Sci. Technol. 38, 4649–4655.

Crittenden, J.C., Sanongraj, S., Bulloch, J.L., Hand, D.W., Rogers, T.N., Speth, T.F., Ulmer, M., 1999. Correlation of aqueous-phase adsorption isotherms. Environ. Sci. Technol. 33, 2926–2933.

Dávalos, J.Z., Roux, M.V., Jiménez, P., 2002. Evaluation of poultry litter as a feasible fuel. Thermochim. Acta 394, 261–266.

de Rudder, J., Van de Wiele, T., Dhooge, W., Comhaire, F., Verstraete, W., 2004. Advanced water treatment with manganese oxide for the removal of 17 alpha-ethinyl estradiol (EE2). Water Res. 38, 184–192.

Funke, A., Ziegler, F., 2010. Hydrothermal carbonization of biomass: a summary and discussion of chemical mechanisms for process engineering. Biofuel Bioprod. Biorefining 4, 160–177.

Glaser, B., Lehmann, J., Zech, W., 2002. Ameliorating physical and chemical properties of highly weathered soils in the tropics with charcoal-A review. Biol. Fertil. Soils 35, 219–230.

Haberhauer, G., Rafferty, B., Strebl, F., Gerzabek, M.H., 1998. Comparison of the composition of forest soil litter derived from three different sites at various decompositional stages using FTIR spectroscopy. Geoderma 83, 331–342.

Hu, J.Y., Chen, X., Tao, G., Kekred, K., 2007. Fate of endocrine disrupting compounds in membrane bioreactor systems. Environ. Sci. Technol. 41, 4097–4102.

Keiluweit, M., Nico, P.S., Johnson, M.G., Kleber, M., 2010. Dynamic molecular structure of plant biomass-derived black carbon (biochar). Environ. Sci. Technol. 44, 1247–1253.

Lehmann, J., Gaunt, J., Rondon, M., 2006. Bio-char sequestration in terrestrial ecosystems – a review. Mitig. Adapt. Strateg. Glob. Change 11, 395–419.

Liang, B., Lehmann, J., Solomon, D., Kinyangi, J., Grossman, J., O'Neill, B., Skjemstad, J.O., Thies, J., Luizao, F.J., Petersen, J., Neves, E.G., 2006. Black carbon increases cation exchange capacity in soils. Soil Sci. Soc. Am. J. 70, 1719–1730.

Liang, B., Lehmann, J., Solomon, D., Sohi, S., Thies, J.E., Skjemstad, J.O., Luizão, F.J., Engelhard, M.H., Neves, E.G., Wirick, S., 2008. Stability of biomass-derived black carbon in soils. Geochim. Cosmochim. Acta 72, 6069–6078.

Nogueira, M.C., Tavares, M.I.B., Nogueira, J., 2004. ^{13}C NMR molecular dynamic investigation of tropical wood agelin pedra (*Hymenolobium paetrum*). Polymer 45, 1217–1222.

Novak, J.M., Lima, I., Xing, B., Gaskin, J.W., Steiner, C., Das, K.C., Ahmedna, M., Rehrah, D., Watts, D.W., Busscher, W.J., Schomberg, H., 2009. Characterization of designer biochar produced at different temperatures and their effects on a loamy sand. Ann. Environ. Sci. 3, 195–206.

Pastorova, I., Botto, R.E., Arisz, P.W., Boon, J.J., 1994. Cellulose char structure: a combined analytical Py-GC–MS, FTIR, and NMR study. Carbohydr. Res. 262, 27–47.

Perlack, R.D., Wright, L.L., Turhallow, A.F., Graham, R.L., Stokes, B.J., Erbach, D.C., 2005. Biomass as a feedstock for a bioenergy and bioproducts industry: the technical feasibility of a billion-ton annual supply. In: U.D. of Energy (DOE/GO-102995-2135). Oak Ridge National Laboratory, Oak Ridge, TN.

Peterson, A.A., Vogel, F., Lachance, R.P., Froling, M., Antal, M.J., Tester, J.W., 2008. Thermochemical biofuel production in hydrothermal media: a review of sub- and supercritical water technologies. Energy Environ. Sci. 1, 32–65.

Paris, O., Zollfrank, C., Zickler, G.A., 2005. Decomposition and carbonisation of wood biopolymers – a microstructural study of softwood pyrolysis. Carbon 43, 53–66.

Ran, Y., Sun, K., Yang, Y., Xing, B., Zeng, E., 2007. Strong sorption of phenanthrene by condensed organic matter in soils and sediments. Environ. Sci. Technol. 41, 3952–3958.

Sander, M., Pignatello, J.J., 2005. Characterization of charchoal adsorption sites for aromatic compounds: insights drawn from single-solute and bi-solute competitive experiments. Environ. Sci. Technol. 39, 1606–1615.

Sohi, S.P., Krull, E., Lopez-Capel, E., Bol, R., 2010. A review of biochar and its use and function in soil. Adv. Agron. 105, 47–82.

Sun, K., Gao, B., Zhang, Z., Zhang, G., Zhao, Y., Xing, B., 2010. Sorption of atrazine and phenanthrene by organic matter fractions in soil and sediment. Environ. Pollut. 158, 3520–3526.

Wang, X., Xing, B., 2007. Sorption of organic contaminants by biopolymer-derived chars. Environ. Sci. Technol. 41, 8342–8348.

Yang, Y., Sheng, G., 2003. Pesticide adsorptivity of aged particulate matter arising from crop residue burns. J. Agric. Food Chem. 51, 5047–5051.

Yu, X.-Y., Ying, G.-G., Kookana, R.S., 2009. Reduced plant uptake of pesticides with biochar additions to soil. Chemosphere 76, 665–671.

Zhu, D., Hyun, S., Pignatello, J.J., Lee, L.S., 2004. Evidence for π–π electron donor–acceptor interactions between π-donor aromatic compounds and π-acceptor sites in soil organic matter through pH effects on sorption. Environ. Sci. Technol. 38, 4361–4368.

Zhu, D., Pignatello, J.J., 2005. Characterization of aromatic compound sorptive interactions with black carbon (charcoal) assisted by graphite as a model. Environ. Sci. Technol. 39, 2033–2041.